The Iranian Journal of Mechanical Engineering Transactions of ISME
Journal homepage: https://jmee.isme.ir/
Vol. 24, No. 2, 2023, pp. 60-80

Research Paper

DOI: https://doi.org/10.30506/jmee.2023.2013978.1325

Investigating the Influence of Piezoelectric Excitation on the Veering Phenomenon Associated with Electrostatically Coupled Micro-beams

Hosein Ali Alam-Hakkakan*
M.Sc. Student

Amir Reza Askari†,‡
Associate Professor

Masoud Tahani§
Professor

This paper introduces piezoelectric excitation as a balancing mechanism for mode-localized mass micro-sensors. To this end, adopting the Hamilton principle together with the Ritz method, the non-linear reduced equations of motion governing electrostatically coupled micro-beams with piezoelectric layers are obtained. The free vibration equations associated with the present system are also extracted by linearizing the motion equations around the previously determined static configuration of the system. Solving the free vibration equations, the eigenvalue loci of the system are then plotted. Afterward, the influence of piezoelectric excitation on the veering phenomenon is studied. The results, whose accuracy is successfully validated by those available in the literature, reveal that piezoelectric excitation can drastically affect the veering phenomenon. For instance, it is observed that the application of the electrostatic voltage of 4V can be compensated by the piezoelectric excitation of -35.4695 mV so that the veering phenomenon will occur at the same coupling voltage. Given this important observation, the possibility of employing piezoelectric excitation in designing tunable resonant mass micro-sensors that operate based on the mode-localization phenomenon suggests itself.

Keywords: Veering phenomenon, Tunable mass sensors, Piezoelectric excitation

*M.Sc. Student, Department of Mechanical Engineering, Ferdowsi University of Mashhad, Mashhad, Iran, aliaalam76@gmail.com
†Associate Professor, Department of Mechanical Engineering, Hakim Sabzevari University, Sabzevar, Iran, ar.askari@hsu.ac.ir
‡Research Fellow, Department of Engineering and Technology, The University of Huddersfield, Huddersfield HD1 3DH, UK, a.askari@hud.ac.uk
§Corresponding Author, Professor, Department of Mechanical Engineering, Ferdowsi University of Mashhad, Mashhad, Iran, mtahani@um.ac.ir

Received: 2023/10/20, Revised: 2023/12/12, Accepted: 2023/12/27

1 Introduction

The acronym of MEMS stands for microelectromechanical systems [1]. MEMS devices generally operate as sensors or actuators [2]. One of the largest categories of MEMS-based sensors is resonant mass micro-sensors [3]. This class of micro-sensors generally refers to a continuous structure at the micron scale such as a micro-beam that obtains the mass of a particle via calculating the shift in the resonance frequency of the device before and after the attachment of a target entity [4]. However, beam-type mass micro-sensors do not enjoy high sensitivity; because adding a particle with an extremely small mass to a micro-beam cannot considerably change its resonance frequency [5-7].

To remove the aforementioned incapability of beam-type mass micro-sensors and design high-sensitive devices, exploiting the mode-localization phenomenon was suggested by Spletzer et al. [5]. The mode-localization phenomenon [8], which was discovered by Anderson [8], refers to the concentration of the vibrational energy in a small geometric region instead of the whole structure [9]. For instance, under the conditions of weak internal coupling, the presence of small irregularities in periodic structures can inhibit the propagation of vibration and lead to the localization of vibration modes [10].

A mode-localized resonant mass micro-sensor generally consists of weakly coupled two identical micro-resonators oscillating at their simultaneous resonance state. According to the concept of mode-localization, when a small particle is attached to one of the micro-resonators and consequently changes its resonance zone, the vibration amplitude of the corresponding resonator is drastically suppressed; because the excitation frequency takes place far away from the resonance zone associated with this resonator [11]. This phenomenon is the main sensing principle in mode-localized resonant mass micro-sensors. Given the fact that adding a small disorder can provide a considerable frequency shift in the resonance zone associated with weakly coupled resonators, it is obvious that the sensitivity of mode-localized mass sensors is extremely more than that of single resonator systems [12].

As mentioned above, the mode localization phenomenon occurs when the system is out of balance (i.e., a small disorder is being applied on one of the two resonators). To find the balance state of the system, one should plot the eigenvalues loci associated with the system versus the disorder parameter [13]. Doing so, a veering phenomenon [14] can be observed in the loci of eigenvalues when the disorder parameter vanishes. It is worth mentioning that for a point far away from the veering zone, the modes of the unbalanced system become strongly localized around the resonator on which the disorder is not applied [15]. This is the reason behind the fact that both the eigenvalue loci veering and mode-localization phenomena occur simultaneously.

Given the advantages associated with the mode-localized mass micro-sensors with variable stiffness, such as environmental adaptability, the design and analysis of electrically actuated sensors motivate the attention of many researchers to date. Exploiting electrical actuation for designing adjustable sensors was first proposed by Thiruvenkatanathan et al. [16]. The authors [17] also reported the first empirical work on the application of mode localization phenomenon in electrically coupled micro-systems. They observed a rapid but continuous interchange of the eigenfunctions during the veering phenomenon. They concluded that the electrical coupling provides the possibility of adjusting the modal interchange severity and, consequently, the extent of energy confinement within the system. In view of the fact that applying electrical actuation can shift the veering point, Walter et al. [18] studied the possibility of using electrical actuation to overcome the manufacturing defects of the system. Zhao et al. [19] investigated the capability of the electrical coupling for tuning of 3-DoF coupled resonators instead of traditional 2-DoF systems. They expressed that the electrical coupling provides more degrees of freedom for tuning the systems when it consists of more resonators. Kacem et al. [20]

designed two mechanically coupled nano-cantilevers with different lengths under electrostatic actuation and internal resonance. In this study, the veering phenomenon was investigated under different values of the length ratio of the resonators. Zhang et al. [21] proposed two weakly coupled resonators subjected to electrical bias that operated in the linear regime. They controlled the initial working point of the system by adjusting the bias voltage applied to the resonators. Rabenimanana et al. [22]designed two electrostatically coupled cantilevers with different lengths. They observed that the difference between the stiffness values of the cantilevers can be compensated by employing the softening effect of electrical actuation. In another study, they showed that the electrostatic tunability magnifies the mode localization effect led to a drastic improvement in the mass sensors' sensitivity [23]. Ilyas et al. [24] calculated the natural frequencies of electrostatically and mechanically coupled micro-beams. They verified their findings experimentally and showed that, despite the electrostatic coupling, the mechanical coupling is not possible to tune significantly the eigenvalues of the system. This is due to the fact that the coupling strength cannot be changed once fabricated. The veering phenomenon associated with the first three vibration modes of a mode-localized system was investigated by Ouakad et al. [25]. It was demonstrated that by controlling the DC voltage, the veering point and their respective localization characteristics can be altered. Lyu et al. [26, 27] studied the combined effects of the electrical actuation and micro-resonators length as well as thickness ratios on the veering point's position of non-linear mode-localized mass sensors. Alkaddour et al. [28] developed a general model for a mode-localized mass sensor made of N weakly coupled resonators subjected to an electrical actuation. They tuned their system by adjusting the DC and AC voltages applied to the system. Zhao et al. [29] analyzed the effect of different eigenmodes coupling on the balance condition of the mode-localized mass sensors. Their proposed model consists of two electrostatically coupled micro-beams with different values of thicknesses subjected to the DC and AC voltages. They showed that the veering point, and consequently the system's equilibrium state, can be changed once the different eigenmodes are coupled with each other.

Bearing in mind that applying DC voltage can only decrease the stiffness of the structure, the idea of exploiting piezoelectric excitation, which can both decrease and increase the stiffness of the system, suggests itself. Therefore, the present work aims to investigate the influence of piezoelectric excitation on the veering phenomenon to provide a tunable mass micro-sensor design with more degrees of freedom. To this end, employing the Euler-Bernoulli beam theory together with the Ritz method, the set of the reduced equations of motion associated with a dual beam mass sensor is obtained. Neglecting the time-dependent terms, the set of reduced equilibrium equations is then extracted and solved numerically using the Newton-Raphson method. The model's predictions for the static configuration of the system are successfully verified through direct comparison with available results in the literature. Afterward, the eigenvalue problem associated with the present system is obtained by linearizing the equations of motion around the previously determined static configuration of the system. Solving the set of the present governing free vibration equations analytically, the eigenvalues loci are obtained. By doing this, the influence of piezoelectric excitation on the veering phenomenon is studied. The main novelties of the present study are

- Modeling electrically coupled micro-beams when they are equipped with piezoelectric layers.
- Providing Ritz-based reduced order model for the system.
- Studying the influence of piezoelectric excitation on static configuration of the system.
- Investigating the coupled electrostatic and piezoelectric excitations on the free vibration behavior of the system, especially on its veering point.
- Introducing the piezoelectric excitation as a mechanism for tuning the balance state of the mode-localized mass micro-sensors.

2 Mathematical model of the problem

The present system consists of two clamped micro-beams, as depicted in Figure (1), which are coupled through the application of a coupling voltage V_c between them. Despite the upper micro-beam (i.e., micro-beam 1) that is made of a homogeneous material, the lower one (i.e., micro-beam 2) is made of two piezoelectric layers symmetrically attached to both sides of a homogeneous substrate. The voltages V_{p1} and V_{p2} are applied to the upper and lower piezoelectric layers, respectively. It is assumed that the length, width, and thickness of the upper micro-beam are *L*, *b*, and *h*, respectively. In addition, the geometric properties associated with the substrate of the lower micro-beam are considered to be the same as those of the upper one. Also, the thicknesses of the piezoelectric layers are taken the same and equal to h_p. The initial gap between the two micro-beams is g_c. In addition, g_a denotes the initial gap between the lower micro-beam and the fixed substrate. Furthermore, *x*, *y*, and *z* are the coordinates along the length, width, and thickness of the upper micro-beam.
According to the Euler–Bernoulli beam theory, the displacement components associated with an arbitrary point of the micro-beam are given by [30]:

$$u_1 = u(x,t) - z\frac{\partial w(x,t)}{\partial x}, \quad u_2 = 0, \quad u_3 = w(x,t), \tag{1}$$

where u and w are the displacements of a point located on the mid-plane of the micro-beam, respectively, in the *x* and *z* directions. Employing the von Kármán strain-displacement relation, the only non-zero strain component of the displacement field given in Equation (1) can be expressed as [30]:

$$\varepsilon_x = \frac{\partial u}{\partial x} + \frac{1}{2}\left(\frac{\partial w}{\partial x}\right)^2 - z\frac{\partial^2 w}{\partial x^2}. \tag{2}$$

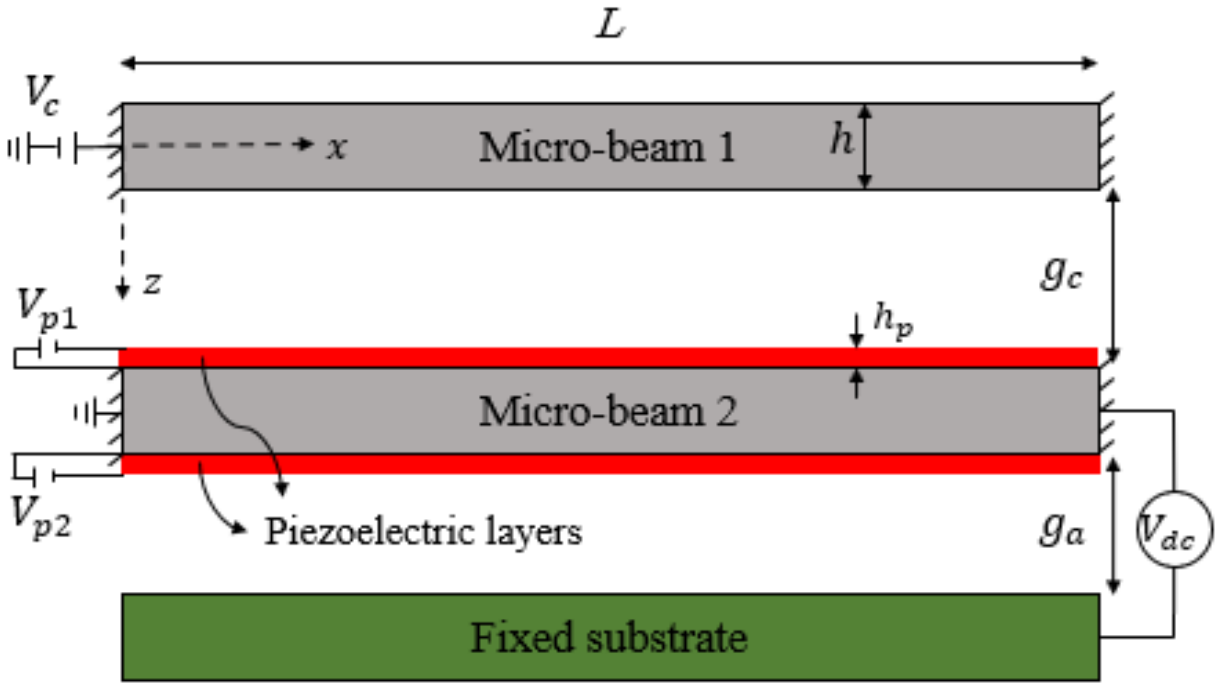

Figure 1 Schematic of the present system

Given the strain-displacement introduced in Equation (2), the variational form of the strain energy expression associated with the i^{th} micro-beam ($i = 1, 2$) is [31]:

$$\delta U_i = \int_{V_i} \sigma_x \delta \varepsilon_x dV_i = b \int_0^L (N_i \delta u_i' + N_i w_i' \delta w_i' - M_i \delta w_i'') dx, \tag{3}$$

where the prime sign denotes differentiation with respect to variable x. Also, V_i refers to the volume of the i^{th} micro-beam ($i = 1, 2$) and $(N_i, M_i) = \int \sigma_x(1, z) dz$ are the corresponding force and moment resultants [31].
Since the lower micro-beam is composed of three layers, as was previously mentioned, the corresponding stress-strain relations are as follows:

$$\sigma_x = \begin{cases} E_p \varepsilon_x + e_{31} V_{p1}/h_p & -(h_p + h/2) \le z \le -h/2 \\ E_s \varepsilon_x & -h/2 \le z \le h/2 \\ E_p \varepsilon_x + e_{31} V_{p2}/h_p & h/2 \le z \le (h/2 + h_p) \end{cases} \tag{4}$$

where E_p, h_p, and e_{31} are the Young's modulus, thickness, and piezoelectric constant of the piezoelectric layers. Also, E_s denotes Young's modulus of the substrates.
The electrostatic attraction between the two micro-beams, which is denoted by F_c, and that exerted on the lower one, which is denoted by F_{es}, per unit length of the beams, can be expressed as [32]:

$$F_c^i = \frac{\varepsilon V_C^2 (-1)^{i+1}}{2(g_c - w_1 + w_2)^2}, \tag{5a}$$

$$F_{es} = \frac{\varepsilon V_{dc}^2}{2(g_a - w_2)^2}, \tag{5b}$$

where $\varepsilon = 8.854 \times 10^{-12}$ (Fm^{-1}) is the dielectric constant of the vacuum [33]. Also, V_{dc} represents the amplitude of the DC voltage applied to the lower micro-beam. In addition, $w_1(x, t)$ and $w_2(x, t)$ are the deflections of the upper and lower micro-beams, respectively.
Given the displacement field introduced in Equation (1), the variational form of the kinetic energy associated with the i^{th} micro-beam ($i = 1, 2$) can be written as [31]:

$$\delta K_i = b\left(2\delta_{i2}\rho_p h_p + \rho_s h\right) \int_0^L (\dot{u}_i \delta \dot{u}_i + \dot{w}_i \delta \dot{w}_i) dx, \tag{6}$$

where the dot sign denotes differentiation with respect to time t. Also, ρ_i is the density of the i^{th} micro-beam ($i = 1, 2$).
It is to be noted that despite the density of the upper micro-beam (i.e., ρ_1) being a constant along its thickness, the one associated with the lower micro-beam (i.e., ρ_2) varies along the thickness of this structure as:

$$\rho_2 = \begin{cases} \rho_p & -(h_p + h/2) \le z \le -h/2 \\ \rho_s & -h/2 \le z \le h/2 \\ \rho_p & h/2 \le z \le (h/2 + h_p) \end{cases} \tag{7}$$

where ρ_p and ρ_s are the densities of the piezoelectric layer and substrate, respectively. Furthermore, the virtual work done by these electrostatic excitations can be written as:

$$(\delta W_c)_i = \int_0^b \int_0^L F_c^i \delta w_i dx dy = \int_0^L \frac{\varepsilon b V_C^2 (-1)^{i+1}}{2(g_c - w_1 + w_2)^2} \delta w_i dx, \tag{8a}$$

$$\delta W_{es} = \int_0^b \int_0^L F_{es} \delta w_2 dx dy = \int_0^L \frac{\varepsilon b V_{dC}^2}{2(g_a - w_2)^2} \delta w_2 dx. \tag{8b}$$

Having the kinetic energy and inertia terms as well as the virtual work done by the electrical actuations, Hamilton's principle can be employed to obtain the equations of motion associated with the system. This principle can be stated as [31]:

$$\int_{t_i}^{t_f} \left(\delta K_i - \delta U_i + \delta W_{ext}^i\right) dt = 0, \tag{9}$$

where δW_{ext}^i $(i = 1, 2)$ refers to the virtual work done by the external forces on the i^{th} micro-beam $(i = 1, 2)$, which are introduced as follows:

$$\delta W_{ext}^i = (\delta W_c)_i + \delta_{i2} \delta W_{es}\,, \tag{10}$$

with δ_{i2} refers to the Kronecker delta.
Given the fact that the clamped boundary condition is the only one utilized in designing mass sensors for practical applications at micron scales [34], this boundary condition is selected in the present work. Taking the clamped boundary conditions, substituting Equations (3), (6), and (8) into Equation (9), solving the displacement u_i in terms of the deflection w_i for the case of clamped boundary conditions and following some straightforward mathematical manipulations, one gets:

$$\int_{t_i}^{t_f} \int_0^L (-b\{\rho_s h + 2\delta_{i2}\rho_p h_p\}\ddot{w}_i \delta w_i + bM_i \delta w_i'' - b\tilde{N}_i w_i' \delta w_i' + \frac{(-1)^{i+1} \varepsilon b V_c^2}{2(g_c - w_1 + w_2)^2} \delta w_i + \frac{\delta_{i2} \varepsilon b V_{dc}^2}{2(g_a - w_2)^2} \delta w_2) dx dt = 0. \tag{11}$$

The introduced stress resultants $\widetilde{N}_i$ and M_i $(i = 1, 2)$ are as follows:

$$\widetilde{N}_i = \frac{(E_s h + 2\delta_{i2} E_p h_p)}{2L} \int_0^L (w_i')^2 dx + \delta_{i2} e_{31}\big(V_{p2} + V_{p1}\big),$$
$$M_i = -\frac{\left(E_s h^3 + 8\delta_{i2} E_p \left(h_p^3 + \frac{3}{2} h_p^2 h + \frac{3}{4} h_p h^2\right)\right) w_i''}{12} + \frac{1}{2}\delta_{i2} e_{31}\big(h_p + h\big)\big(V_{p2} - V_{p1}\big). \tag{12}$$

For convenience, the mechanical energy of the system in Equation (11) is normalized using the following dimensionless variables:

$$\hat{x} = \frac{x}{L}\,, \widehat{w}_1 = \frac{w_1}{g_a}, \widehat{w}_2 = \frac{w_2}{g_a}\,, \hat{t} = \frac{t}{\tau}\,, R = \frac{g_c}{g_a}, \tag{13}$$

Where

$$\tau = \sqrt{\frac{12\rho_s L^4}{E_s h^2}}. \tag{14}$$

Upon substitution of the dimensionless quantities introduced in Equation (13) into Equation (11) and *dropping the hats*, the normalized mechanical energy associated with the present system is obtained as:

$$\int_{t_i}^{t_f} \int_0^1 \{(1 + \delta_{i2}\alpha_3)\ddot{w}_i \delta w_i + (\delta_{i1} + \delta_{i2}\alpha_4) w_i'' \delta w_i'' + (\delta_{i1}\alpha_1 + \delta_{i2}\alpha_5)\left(\int_0^1 (w_i')^2 dx\right) w_i' \delta w_i'$$
$$-\delta_{i2}\alpha_6\big(V_{p2} - V_{p1}\big)\delta w_2'' + \delta_{i2}\alpha_7\big(V_{p2} + V_{p1}\big) w_2' \delta w_2' - \frac{(-1)^{i+1}\alpha_2 V_c^2}{(R - w_1 + w_2)^2}\delta w_i \tag{15}$$
$$-\delta_{i2}\frac{\alpha_2 V_{dc}^2}{(1 - w_2)^2}\delta w_2\Big\}\tau L dt dx = 0\,,$$

in which, the normalized parameters of the system are given by:

$$\alpha_1 = \frac{6g_a^2}{h^2}, \alpha_2 = \frac{6\varepsilon L^4}{E_s h^3 g_a^3}\,, \alpha_3 = \frac{2\rho_p h_p}{\rho_s h}, \alpha_4 = \frac{\left(8E_p h_p^3 + 12E_p h_p^2 h + 6E_p h_p h^2 + E_s h^3\right)}{E_s h^3},$$
$$\alpha_5 = \frac{6g_a^2\left(2E_p h_p + E_s h\right)}{E_s h^3}, \alpha_6 = \frac{6L^2\left(h_p + h\right)}{E_s h^3 g_a} e_{31},\ \alpha_7 = \frac{12L^2}{E_s h^3} e_{31}\,. \tag{16}$$

Using the Ritz method, the deflections of micro-beams are discretized as:

$$w_1(x,t) = \sum_{i=1}^{n} \varphi_i(x) q_{s1,i} + \sum_{j=1}^{N} \varphi_j(x) q_{d1,j}(t), \tag{17a}$$

$$w_2(x,t) = \sum_{i=1}^{n} \varphi_i(x) q_{s2,i} + \sum_{j=1}^{N} \varphi_j(x) q_{d2,j}(t), \tag{17b}$$

where $q_{s1,i}$, $q_{s2,i}$, are the i^{th} static generalized coordinates associated with the upper and lower micro-beams, respectively. In addition, $q_{d1,j}(t)$ and $q_{d2,j}(t)$ are their corresponding dynamic generalized coordinates. Also, φ_j is the j^{th} linear un-damped mode-shape of a clamped beam, which is given by [35]:

$$\varphi_j(x) = \left(\cos(\beta_j x) - \cosh(\beta_j x)\right) - \frac{\cos(\beta_j x) - \cosh(\beta_j x)}{\sin(\beta_j x) - \sinh(\beta_j x)} \left(\sin(\beta_j x) - \sinh(\beta_j x)\right), \tag{18}$$

where $\beta_j(x)$ is the j^{th} eigenvalue of the clamped beam [35], as listed in Table (1).
Next, substituting Equations (17) into Equations (15) and integrating the outcome from $x = 0$ to 1, the present reduced order model is obtained as follows:

$$\sum_{j=1}^{N} \Bigg\{ K_1 \ddot{q}_{d1,j} + K_2\left(q_{s1,i} + q_{d1,j}\right) + \alpha_1 \Bigg(\int_0^1 \left(\sum_{i=1}^{n} \varphi_i' q_{s1,i} \right)^2 + 2 \left\{ \sum_{i=1}^{n} K_3 q_{s1,i} \right\} q_{d1,j} \Bigg) \times K_3\left(q_{s1,i} + q_{d1,j}\right) - \alpha_2 V_c^2 \left(I_1 + 2 I_2 \left(q_{d1,j} - q_{d2,j}\right) \right) \Bigg\} \delta q_{1,j} = 0 \tag{19a}$$

$$\sum_{j=1}^{N} \Bigg\{ \{1+\alpha_3\} K_1 \ddot{q}_{d2,j} + \alpha_4 K_2\left(q_{s2,i} + q_{d2,j}\right) + \alpha_5 \Bigg(\int_0^1 \left(\sum_{i=1}^{n} \varphi_i' q_{s2,i} \right)^2 + 2 \left\{ \sum_{i=1}^{n} K_3 q_{s2,i} \right\} q_{d2,j} \Bigg) \times K_3\left(q_{s2,i} + q_{d2,j}\right) - \alpha_6 \left(V_{p2} - V_{p1}\right) K_4 + \alpha_7 \left(V_{p2} + V_{p1}\right) \times K_3\left(q_{s2,i} + q_{d2,j}\right) - \alpha_2 V_{dc}^2 \left(I_3 + 2 I_4 q_{d2,j}\right) + \alpha_2 V_c^2 \left(I_1 + 2 I_2 \left(q_{d1,j} - q_{d2,j}\right) \right) \Bigg\} \delta q_{2,j} = 0 \tag{19b}$$

where all the introduced coefficients in this equation are given in Appendix A. It is worth mentioning that the static configuration of the system under the action of the electrical actuations can be determined by the solution of the reduced equilibrium equation that can simply be obtained by neglecting the time-dependent terms in Equations (19).

Table 1 The eigenvalues of the clamped beam [35]

β_1	β_2	β_3
4.7300	7.8532	10.9956

These non-linear algebraic equations will be solved numerically through the use of the Newton-Raphson procedure in this paper.
Having the static configuration of the present system, the free vibration equations can be obtained by linearizing the present system of initial value problems (IVPs) given in Equations (19) around the pre-determined static configuration as:

$$\ddot{q}_{d1,j} + (K_2 + 2\alpha_1 S_1^2 + \alpha_1 S_2 K_3 - 2\alpha_2 V_c^2 I_2) q_{d1,j} + 2\alpha_2 V_c^2 I_2 q_{d2,j} = 0, \tag{20a}$$

$$\begin{aligned} \{1+\alpha_3\}\ddot{q}_{d2,j} + \{\alpha_4 K_2 + 2\alpha_5 S_3^2 + \alpha_5 S_4 K_3 + \alpha_7 (V_{p2} + V_{p1}) K_3 \\ -2\alpha_2 V_c^2 I_2 - 2\alpha_2 V_{dc}^2 I_4\} q_{d2,j} + 2\alpha_2 V_c^2 I_2 q_{d2,j} = 0. \end{aligned} \tag{20b}$$

Assuming simple harmonic motion for the dynamic counterpart of generalized coordinates of the micro-beams (i.e., $q_{d1,j}$ and $q_{d2,j}$), the set of eigenvalue-eigenvector equations can be written as:

$$\begin{bmatrix} R_{11} - \Omega_n^2 & R_{12} \\ R_{21} & R_{22} - \Omega_n^2\{1+\alpha_3\} \end{bmatrix} \begin{Bmatrix} Q_{d1,j} \\ Q_{d2,j} \end{Bmatrix} = \begin{Bmatrix} 0 \\ 0 \end{Bmatrix}, \tag{21}$$

where Ω_n is the natural frequency and $Q_{d1,j}$ and $Q_{d2,j}$ are the eigenvectors. In addition, the introduced coefficients in Equation (21) are given in Appendix B.
Solving this set of eigenvalue-eigenvector equations, the combined effects of the electrostatic and piezoelectric excitations on the static configuration of the system and veering phenomenon will be investigated in the next section.

3 Results and discussion

3.1 Validation of system

To validate the presented model, neglecting the influence of the upper micro-beam (i.e., setting $V_c = 0$), pull-in voltages associated with a single beam equipped with piezoelectric layers are compared to those presented in the literature.
To this end, a bimorph micro-beam with geometric and material properties, respectively, given in Tables (2) and (3), is considered.
Assuming the upper and lower piezoelectric layers are excited by a similar voltage, Figure (2) illustrates the variation of the pull-in voltage of the system versus the piezoelectric voltage.As it is seen, there exist excellent agreements between the present results and those reported by Rezazadeh et al. [36]. It is worth mentioning that the substrate and the piezoelectric layers are assumed to be made of Silicon and PZT-4, respectively. Also, the value of the initial gap is set to 1 μm (i.e., $g_a = 1\mu m$).
This section explores the effect of the piezoelectric excitation on the static configuration of the system. To this end, the present electrostatically coupled system, whose lower micro-beam has been equipped with two PZT-4 layers, is considered. The geometric properties of the system are assumed to be the same as those given in Table (4). It is noteworthy that similar voltages are applied across the piezoelectric layers. Also, the electrostatic coupling voltage between the two micro-beams is set to $V_c = 2\,V$.

Table 2 Geometric properties of the substrate and piezoelectric layers [36]

	L(μm)	b(μm)	h(μm)
Substrate	350	50	3
Piezoelectric layers	350	50	0.01

Table 3 Material properties of the substrate and piezoelectric layers [36]

	E(GPa)	ρ(Kg/m^3)	e_{31}
Silicon	169	2331	-
PZT-4	78.6	7500	-9.29

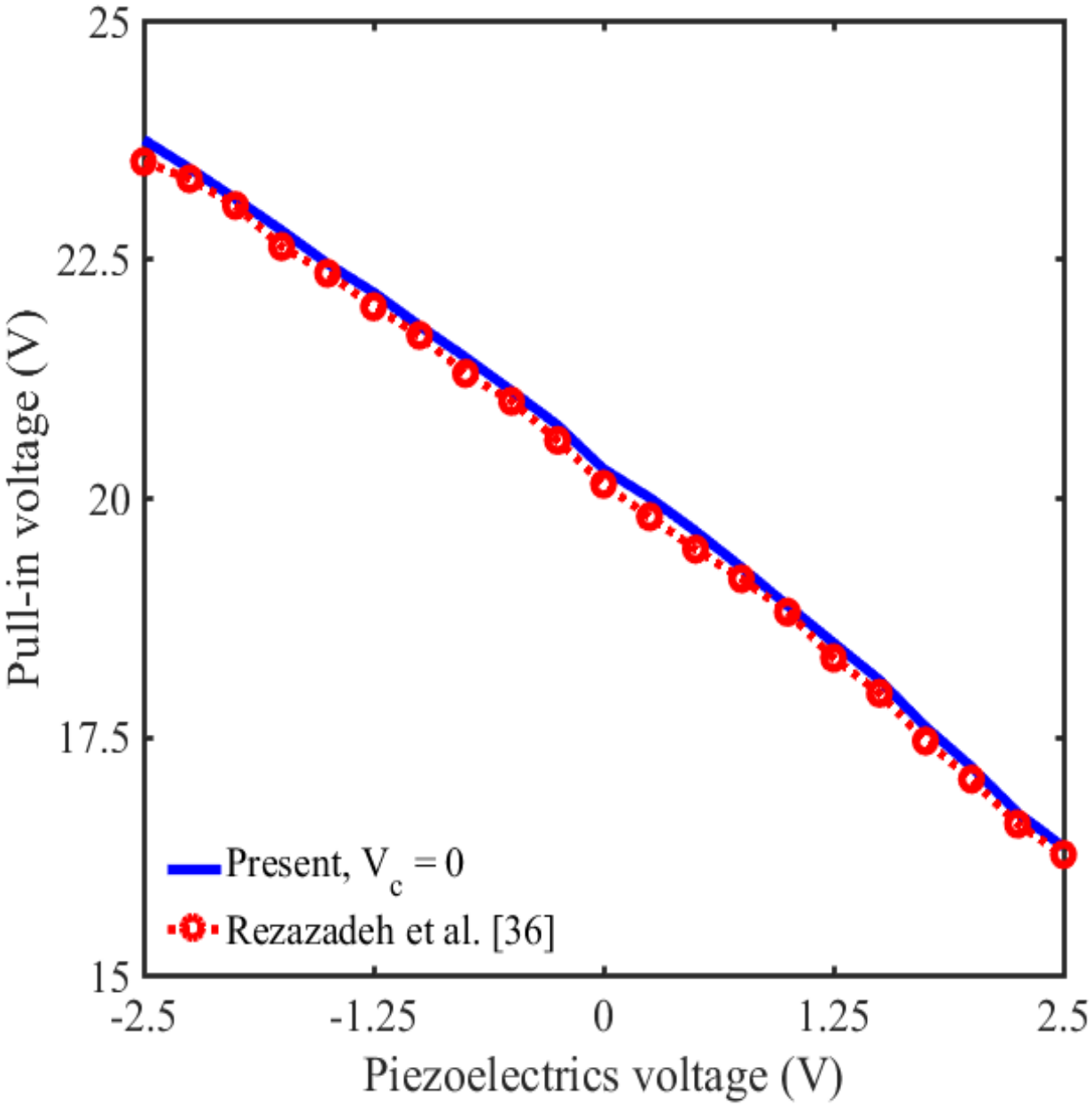

Figure 2 Pull-in voltages versus piezoelectric voltages for a system with properties presented in Tables (2) and (3)

3.2 Static analysis

This section explores the effect of the piezoelectric excitation on the static configuration of the system. To this end, the present electrostatically coupled system, whose lower micro-beam has been equipped with two PZT-4 layers, is considered. The geometric properties of the system are assumed to be the same as those given in Table (4). It is noteworthy that similar voltages are applied across the piezoelectric layers. Also, the electrostatic coupling voltage between the two micro-beams is set to $V_c = 2\,V$.

Table 4 Geometric properties of the electrostatically coupled system with two piezoelectric layers

	L(μm)	b(μm)	h(μm)
Substrate	210	4	1
Piezoelectric layers	210	4	0.005

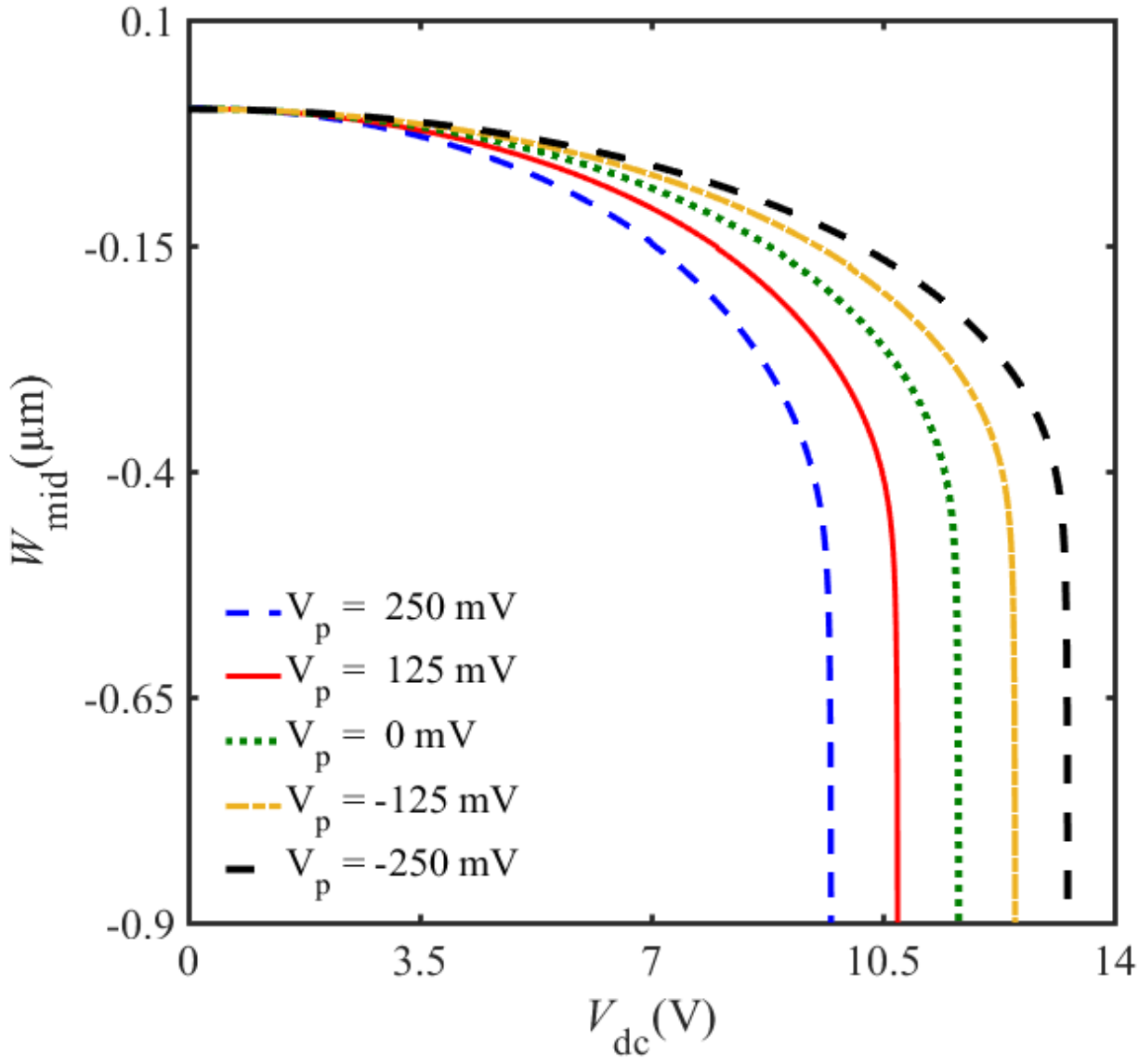

Figure 3 Equilibrium path of the lower micro-beam for different values of piezoelectric voltages. The system properties are listed in Tables (3) and (4) and the coupling voltage is adjusted to $V_c = 2\,V$

The equilibrium path of the lower micro-beam versus the applied DC voltage for different values of the piezoelectric voltages is illustrated in Figure (3). According to this figure, the piezoelectric excitation has a significant impact on the static configuration of the system. Also, the occurrence of pull-in instability can be controlled by adjusting the piezoelectric voltage. It can be observed that applying a negative voltage to the piezoelectric layers increases the pull-in voltage. The reason behind this fact is that the negative piezoelectric voltage applies a tensile force on the lower micro-beam and so increases its stiffness, leading to the increase in its pull-in threshold.

3.3 Mode veering analysis

The influence of the piezoelectric excitation and the electrostatic coupling between two micro-beams on the veering phenomenon will be studied in this section. The present electrostatically coupled system with properties presented in Tables (3) and (4) is considered again.
The variation of the system eigenvalues versus the piezoelectric voltage as the disorder parameter (i.e., the eigenvalues loci) is plotted in Figure (4) to find the balance state of the system. It is assumed that the electrostatic voltage is set to $V_{dc} = 4\ V$.

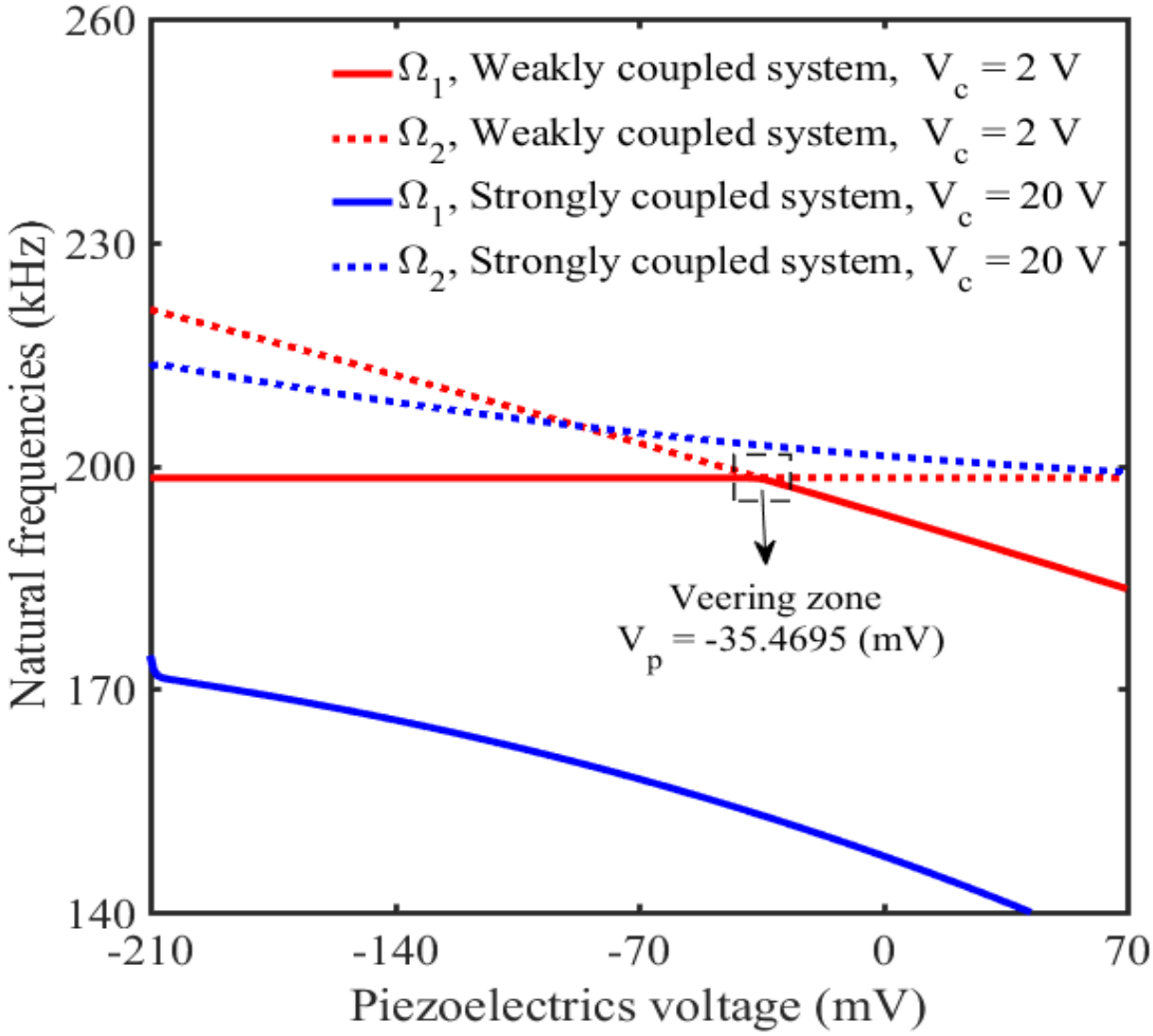

Figure 4 Eigenvalues loci for systems with two different coupling voltages. The electrostatic actuation is set to $V_{dc} = 4\ V$ and the properties are assumed to be as those given in Tables (3) and (4)

Figure (4) presents the results for two different coupling voltages. As depicted in the figure, a small coupling voltage leads to the occurrence of the veering phenomenon.
As Figure (4) shows, only weakly coupled systems can face the veering phenomenon. To investigate this issue more, Table (5) represents the eigenvectors associated with the eigenvalues depicted in Figure (4). That is, $W_{mid}^{11}/W_{mid}^{21}$ denotes the ratio of the upper to lower micro-beam mid-point deflection corresponding to the first eigenvalue and $W_{mid}^{12}/W_{mid}^{22}$ is the one associated with the second eigenvalue. Hence, $W_{mid}^{11}/W_{mid}^{21}$ and $W_{mid}^{12}/W_{mid}^{22}$ are the first and the second eigenvectors of the system, respectively, for regions before the veering zone. Also, $W_{mid}^{11}/W_{mid}^{21}$ and $W_{mid}^{12}/W_{mid}^{22}$ denote the second and the first eigenvectors for regions beyond this zone. It is obvious that $W_{mid}^{11}/W_{mid}^{21}$ and $W_{mid}^{12}/W_{mid}^{22}$ for strongly coupled systems refer to its first and second eigenvector all the time.

Table 5 Eigenvectors associated with the different situations observed in Figure (4)

V_p(mV)	V_c = 2V		V_c = 20V	
	$W_{mid}^{11}/W_{mid}^{21}$	$W_{mid}^{12}/W_{mid}^{22}$	$W_{mid}^{11}/W_{mid}^{21}$	$W_{mid}^{12}/W_{mid}^{22}$
-108	-86.4629	0.0119	-1.0819	0.9540
-72	-43.6038	0.0237	-0.9368	1.1018
-35.4695	-1.0159	1.0160	-0.8126	1.2702
0	42.4254	-0.0243	-0.7125	1.4487
36	85.5492	-0.0121	-0.6288	1.6416

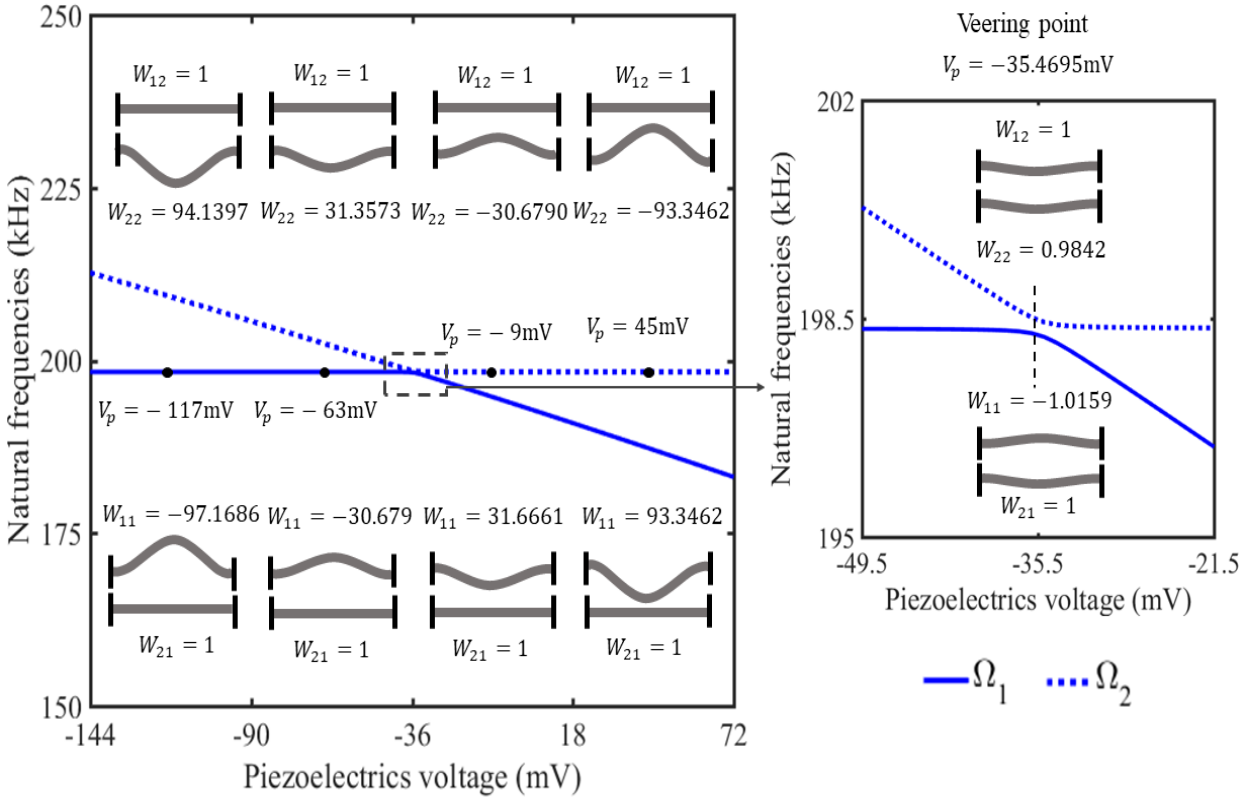

Figure 5 Micro-beams configurations for the present weakly coupled system with $V_c = 2\ V$ and $V_{dc} = 4\ V$ whose eigenvalue loci has been given in Figure (4)

As Table (5) illustrates, despite the strongly coupled systems, the vibration modes are localized by getting away from the veering point in weakly coupled systems. Furthermore, it is seen that neglecting the sign, both the eigenvectors take the same values at the veering point. This means that both the vibration modes of the system are excited simultaneously. Therefore, if one excites a system with a frequency close to that associated with its veering point, both the eigenmodes of the system will experience the resonance phenomenon.

As mentioned above, getting away from the veering point makes the vibration mode to be localized around one of the micro-beams. To investigate this issue more, Figure (5) illustrates each micro-beam configuration at some points of eigenvalue loci presented in Figure (4). According to the results shown in this figure, when the system deviates from its balanced state, where both the upper and lower micro-beams are oscillating, the vibration mode becomes localized around one of the micro-beams. This means that the vibrations of the other resonator are suppressed.

Figure (5) demonstrates that both the upper and lower micro-beams oscillate at the balance state. However, deviating from the balance state, for instance, adding a mass on the upper micro-beam as the external disorder, results in the drastic suppression of the vibrations of this resonator. These drastic changes in the vibrations of the upper micro-beam can be employed as the sensing principle in mode-localized mass micro-sensors.

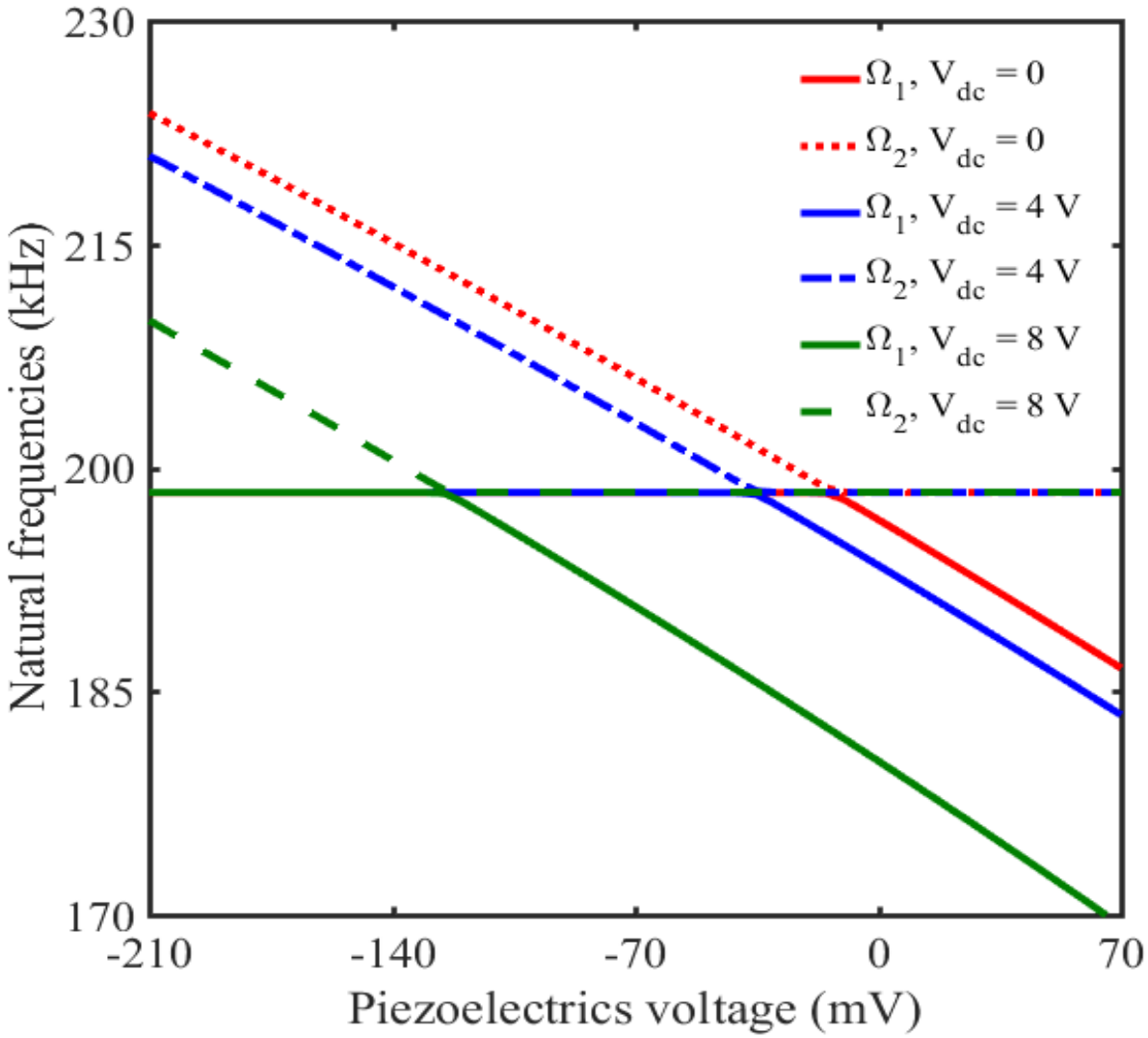

Figure 6 Combined influences of the electrical actuation and the piezoelectric excitation on the eigenvalues loci associated with the present weakly coupled system with $V_c = 2\,V$ and other properties given in Tables (3) and (4)

As mentioned in the introduction section, the present system offers more degrees of freedom compared to existing designs in the literature. This allows for the utilization of a combination of electrical actuation and piezoelectric excitation to tune the system. Regarding this issue, Figure (6) investigates the combined effects of electrical and piezoelectric actuations. As this figure depicts, applying DC voltage shifts the veering point to the left. The reason behind this observation is that applying electrical attraction reduces the stiffness of the system which needs to be compensated by increasing the piezoelectric actuation. As seen, the utilization of a combination of piezoelectric and electrostatic actuations offers increased degrees of freedom for designing tunable, mode-localized mass micro-sensors.

4 Conclusions

The main goal of the present work was to study the effect of piezoelectric excitation on the free vibration characteristics associated with tunable mode-localized mass micro-sensors. To this end, employing the Hamilton principle together with the Ritz method, the reduced equations of motion were obtained. Determining the static deflection of the system under the action of the electrical actuation, the eigenvalue problem governing the free vibrations of the system around its static configuration was obtained. The combined effects of the electrical and piezoelectric excitations on the eigenvalue loci of the system were studied and validated with those available in the literature. The results revealed that the piezoelectric excitation has a significant effect on the stiffness of the structure. Therefore, the static configuration of the system and the occurrence of pull-in instability can be controlled by adjusting the piezoelectric voltage. In the rest of the paper, investigating the influence of the coupling voltage showed that only weakly coupled systems can face veering and consequently mode-localization phenomena. It was found that employing piezoelectric actuation can compensate for the reductive effect of the electrical excitation on the stiffness of the system. Therefore, it was observed that piezoelectric-based systems can potentially suggest more degrees of freedom in the design procedure of mode-localized mass micro-sensors.

Conflict of interest: The authors declare that they have no known competing financial interests or personal relationships that could have appeared to influence the work reported in this paper.

References

[1] M. I. Younis, "MEMS Linear and Nonlinear Statics and Dynamics." USA: Springer, 2011, doi: https://doi.org/10.1007/978-1-4419-6020-7.

[2] H. A. Aalam Hakkakan and A. R. Askari, "Non-linear Analysis of FG Beam-based Double-movable-electrode MEMS," (In Persian), *Journal of Solid and Fluid Mechanics,* Vol. 10, No. 2, pp. 111-126, 2020, doi: https://doi.org/10.22044/jsfm.2020.9137.3069.

[3] C. Zhao *et al.*, "A Review on Coupled MEMS Resonators for Sensing Applications Utilizing Mode Localization," *Sensors and Actuators A: Physical,* Vol. 249, pp. 93-111, 2016, doi: https://doi.org/10.1016/j.sna.2016.07.015.

[4] F. Lochon, I. Dufour, and D. Rebière, "An Alternative Solution to Improve Sensitivity of Resonant Microcantilever Chemical Sensors: Comparison between using High-order Modes and Reducing Dimensions," *Sensors and Actuators B: Chemical,* Vol. 108, No. 1, pp. 979-985, 2005, doi: https://doi.org/10.1016/j.snb.2004.11.086.

[5] M. Spletzer *et al.*, "Ultrasensitive Mass Sensing using Mode Localization in Coupled Microcantilevers," *Applied Physics Letters*, Vol. 88, No. 25, 2006, doi: https://doi.org/10.1063/1.2216889.

[6] A. R. Askari and M. Tahani, "Investigating Nonlinear Vibration of a Fully Clamped Nanobeam in Presence of the van der Waals Attraction," *Applied Mechanics and Materials*, Vol. 226, pp. 181-185, 2012, doi: https://doi.org/10.4028/www.scientific.net/AMM.226-228.181.

[7] J. Khaghanifard, A. R. Askari, and M. Taghizadeh, "Frequency-domain Analysis of Shock-excited Magneto-electro-elastic Energy Harvesters with Different Unimorph and Bimorph Configurations," *Iranian Journal of Science and Technology, Transactions of Mechanical Engineering*, Vol. 47, No. 3, pp. 1205-1222, 2023, doi: https://doi.org/10.1007/s40997-022-00575-0.

[8] P. W. Anderson, "Absence of Diffusion in Certain Random Lattices," *Physical Review*, Vol. 109, No. 5, pp. 1492-1505, 1958, doi: https://doi.org/10.1103/PhysRev.109.1492.

[9] C. Pierre and E. H. Dowell, "Localization of Vibrations by Structural Irregularity," *Journal of Sound and Vibration*, Vol. 114, No. 3, pp. 549-564, 1987, doi: https://doi.org/10.1016/S0022-460X(87)80023-8.

[10] M. S. Triantafyllou and G. S. Triantafyllou, "Frequency Coalescence and Mode Localization Phenomena: A geometric Theory," *Journal of Sound and Vibration*, Vol. 150, No. 3, pp. 485-500, 1991, doi: https://doi.org/10.1016/0022-460X(91)90899-U.

[11] P. Thiruvenkatanathan and A. Seshia, "Mode-localized Displacement Sensing," *Journal of Microelectromechanical Systems*, Vol. 21, No. 5, pp. 1016-1018, 2012, doi: https://doi.org/10.1109/JMEMS.2012.2198047.

[12] M. Spletzer *et al.*, "Highly Sensitive Mass Detection and Identification using Vibration Localization in Coupled Microcantilever Arrays," *Applied Physics Letters*, Vol. 92, No. 11, 2008, doi: https://doi.org/10.1063/1.2899634.

[13] O. Giannini and A. Sestieri, "Experimental Characterization of Veering Crossing and lock-in in Simple Mechanical Systems," *Mechanical Systems and Signal Processing*, Vol. 72-73, pp. 846-864, 2016, doi: https://doi.org/10.1016/j.ymssp.2015.11.012.

[14] A. W. Leissa, "On a Curve Veering Aberration," *Zeitschrift für Angewandte Mathematik und Physik ZAMP*, Vol. 25, No. 1, pp. 99-111, 1974, doi: https://doi.org/10.1007/BF01602113.

[15] C. Pierre, "Mode Localization and Eigenvalue Loci Veering Phenomena in Disordered Structures," *Journal of Sound and Vibration*, Vol. 126, No. 3, pp. 485-502, 1988, doi: https://doi.org/10.1016/0022-460X(88)90226-X.

[16] P. Thiruvenkatanathan *et al.*, "Enhancing Parametric Sensitivity in Electrically Coupled MEMS Resonators," *Journal of Microelectromechanical Systems*, Vol. 18, No. 5, pp. 1077-1086, 2009, doi: https://doi.org/10.1109/JMEMS.2009.2025999.

[17] P. Thiruvenkatanathan *et al.*, "Manipulating Vibration Energy Confinement in Electrically Coupled Microelectromechanical Rresonator Arrays," *Journal of Microelectromechanical Systems,* Vol. 20, No. 1, pp. 157-164, 2011, doi: https://doi.org/10.1109/JMEMS.2010.2090501.

[18] V. Walter *et al.*, "Electrostatic Actuation to Counterbalance the Manufacturing Defects in a MEMS Mass Detection Sensor using Mode Localization," *Procedia Engineering,* Vol. 168, pp. 1488-1491, 2016, doi: https://doi.org/10.1016/j.proeng.2016.11.431.

[19] C. Zhao *et al.*, "A Force Sensor Based on Three Weakly Coupled Resonators with Ultrahigh Sensitivity," *Sensors and Actuators A: Physical,* Vol. 232, pp. 151-162, 2015, doi: https://doi.org/10.1016/j.sna.2015.05.011.

[20] N. Kacem *et al.*, "Mode Veering and Internal Resonance in Mechanically Coupled Nanocantilevers under Electrostatic Actuation," *Procedia Engineering,* Vol. 168, pp. 924-928, 2016, doi: https://doi.org/10.1016/j.proeng.2016.11.307.

[21] H. Zhang *et al.*, "Linear Sensing for Mode-localized Sensors," *Sensors and Actuators A: Physical,* Vol. 277, pp. 35-42, 2018, doi: https://doi.org/10.1016/j.sna.2018.05.006.

[22] T. Rabenimanana *et al.*, "Mass Sensor using Mode Localization in Two Weakly Coupled MEMS Cantilevers with Different Lengths: Design and Experimental Model Validation," *Sensors and Actuators A: Physical,* Vol. 295, pp. 643-652, 2019, doi: https://doi.org/10.1016/j.sna.2019.06.004.

[23] T. Rabenimanana *et al.*, "Functionalization of Electrostatic Nonlinearities to Overcome Mode Aliasing Limitations in the Sensitivity of Mass Microsensors Based on Energy Localization," *Applied Physics Letters,* Vol. 117, No. 3, 2020, doi: https://doi.org/10.1063/5.0007446.

[24] S. Ilyas and M. I. Younis, "Theoretical and Experimental Investigation of Mode Localization in Electrostatically and Mechanically Coupled Microbeam Resonators," *International Journal of Non-linear Mechanics,* Vol. 125, p. 103516, 2020, doi: https://doi.org/10.1016/j.ijnonlinmec.2020.103516.

[25] H. M. Ouakad, S. Ilyas, and M. I. Younis, "Investigating Mode Localization at Lower- and Higher-order Modes in Mechanically Coupled MEMS Resonators," *Journal of Computational and Nonlinear Dynamics,* Vol. 15, No. 3, 2020, doi: https://doi.org/10.1115/1.4045634.

[26] M. Lyu *et al.*, "Exploiting Nonlinearity to Enhance the Sensitivity of Mode-localized Mass Sensor Based on Electrostatically Coupled MEMS Resonators," *International Journal of Non-linear Mechanics,* Vol. 121, p. 103455, 2020, doi: https://doi.org/10.1016/j.ijnonlinmec.2020.103455.

[27] M. Lyu *et al.*, "Computational Investigation of High-order Mode Localization in Electrostatically Coupled Microbeams with Distributed Electrodes for High Sensitivity Mass Sensing," *Mechanical Systems and Signal Processing,* Vol. 158, p. 107781, 2021, doi: https://doi.org/10.1016/j.ymssp.2021.107781.

[28] M. Alkaddour, M. Ghommem, and F. Najar, "Nonlinear Analysis and Effectiveness of Weakly Coupled Microbeams for Mass Sensing Applications," *Nonlinear Dynamics,* Vol. 104, No. 1, pp. 383-397, 2021, doi: https://doi.org/10.1007/s11071-021-06298-2.

[29] J. Zhao *et al.*, "An Asymmetric Mode-localized Mass Sensor Based on the Electrostatic Coupling of Different Structural Modes with Distributed Electrodes," *Nonlinear Dynamics,* Vol. 108, No. 1, pp. 61-79, 2022, doi: https://doi.org/10.1007/s11071-021-07189-2.

[30] J. N. Reddy, "Theory and Analysis of Elastic Plates and Shells." USA: CRC Press, 2006, doi: https://doi.org/10.1201/9780849384165.

[31] J. N. Reddy, "Energy Principles and Variational Methods in Aapplied Mechanics." USA: John Wiley & Sons, 2017, ISBN: 978-1-119-08737-3.

[32] R. C. Batra, M. Porfiri, and D. Spinello, "Vibrations of Narrow Microbeams Predeformed by an Electric Field," *Journal of Sound and Vibration,* Vol. 309, No. 3, pp. 600-612, 2008, doi: https://doi.org/10.1016/j.jsv.2007.07.030.

[33] D. Chen *et al.*, "Ultrasensitive Resonant Electrometry Utilizing Micromechanical Oscillators," *Physical Review Applied,* Vol. 14, No. 1, p. 014001, 2020, doi: https://doi.org/10.1103/PhysRevApplied.14.014001.

[34] M. I. Younis and F. Alsaleem, "Exploration of New Concepts for Mass Detection in Electrostatically-actuated Structures Based on Nonlinear Phenomena," *Journal of Computational and Nonlinear Dynamics,* Vol. 4, No. 2, 2009, doi: https://doi.org/10.1115/1.3079785.

[35] S. S. Rao, "Vibration of Continuous Systems." USA: John Wiley & Sons, 2019, doi: https://doi.org/10.1002/9781119424284.

[36] G. Rezazadeh, A. Tahmasebi, and M. Zubstov, "Application of Piezoelectric Layers in Electrostatic MEM Actuators: Controlling of Pull-in Voltage," *Microsystem Technologies,* Vol. 12, No. 12, pp. 1163-1170, 2006, doi: https://doi.org/10.1007/s00542-006-0245-5.

Nomenclature

English symbols

b	Width of the micro-beams
E_p	The Young's modulus of the piezoelectric layers
E_s	The Young's modulus of the micro-beams' substrate
F_c	Electrostatic attraction between the upper and lower micro-beams
F_{es}	Electrostatic attraction between the lower micro-beam and the fixed electrode underneath it
g_c	Initial gap between the upper and lower micro-beams
g_a	Initial gap between the lower micro-beam and the fixed electrode underneath it
h	Thickness of the micro-beams' substrate
h_p	Thickness of the piezoelectric layers
K_i	Kinetic energy of the i^{th} micro-beam (i =1,2)
L	Length of the micro-beams
M_i	Moment resultant of the i^{th} micro-beam (i =1,2)
N_i	Force resultant of the i^{th} micro-beam (i =1,2)
$q_{s1,i}$	Static counterpart of the i^{th} (i = 1, 2, 3, ...) generalized coordinate of the upper micro-beam in the Ritz procedure
$q_{s2,i}$	Static counterpart of the i^{th} (i = 1, 2, 3, ...) generalized coordinate of the lower micro-beam in the Ritz procedure
$q_{d1,j}(t)$	Dynamic counterpart of the j^{th} (j = 1, 2, 3, ...) generalized coordinate of the upper micro-beam in the Ritz procedure
$q_{d2,j}(t)$	Dynamic counterpart of the j^{th} (j = 1, 2, 3, ...) generalized coordinates of the lower micro-beam in the Ritz procedure
t	Time
U_i	Strain energy expression of the i^{th} micro-beam (i =1,2)
u_i	Displacements of a point located on the mid-plane of the i^{th} micro-beam (i =1,2) in the x direction
u_1	Displacement component of an arbitrary point of the micro-beam cross section along the x-direction
u_2	Displacement component of an arbitrary point of the micro-beam cross section along the y-direction
u_3	Displacement component of an arbitrary point of the micro-beam cross section along the z-direction
V_i	The volume of the i^{th} micro-beam (i =1,2)
V_{p1}	Piezoelectric voltage of the upper piezoelectric layer
V_{p2}	Piezoelectric voltage of the lower piezoelectric layer
V_{dc}	DC voltage
V_c	Coupling voltage
W_{ext}^i	The work done by the external forces on the i^{th} micro-beam (i =1,2)

W_c	The work done by electrostatic attraction between the upper and lower micro-beams
W_{es}	The work done by electrostatic attraction between the lower micro-beam and the fixed electrode underneath it
$w_1(x,t)$	Deflections of the upper micro-beam
$w_2(x,t)$	Deflections of the lower micro-beam
w_i	Displacements of a point located on the mid-plane of the i^{th} micro-beam (i =1,2) in the *z*-direction
x	*x*-coordinate along the length of the micro-beam
y	*y*-coordinates along the width of the micro-beam
z	*z*-coordinates along the thickness of the micro-beam

Greek symbols

$\beta_j(x)$	j^{th} (j = 1, 2, 3, ...) eigenvalue of the clamped beam
δ	Variational operator
δ_{i2}	Kronecker delta
ε	Dielectric constant of the vacuum
ε_x	Axial strain in the *x* direction
e_{31}	Piezoelectric constant
ρ_p	Density of the piezoelectric layer
ρ_s	Density of the micro-beams' substrate
σ_x	Normal stress in the *x* direction
$\varphi_j(x)$	j^{th} (j = 1, 2, 3, ...) linear un-damped mode-shape of a clamped beam
Ω_1	First natural frequency of the system
Ω_2	Second natural frequency of the system

Appendix A

The coefficients appearing in Equations (19) are defined as:

$$K_1 = \int_0^1 \varphi_j^2 dx\ ,\quad K_2 = \int_0^1 \varphi_j'' \varphi_i'' dx\ ,\quad K_3 = \int_0^1 \varphi_j' \varphi_i' dx,\quad K_4 = \int_0^1 \varphi_j'' dx$$

$$I_1 = \int_0^1 \frac{\varphi_j dx}{\left(R - \sum_{i=1}^n \varphi_i q_{s1,i} + \sum_{i=1}^n \varphi_i q_{s2,i}\right)^2},\quad I_2 = \int_0^1 \frac{\varphi_j^2 dx}{\left(R - \sum_{i=1}^n \varphi_i q_{s1,i} + \sum_{i=1}^n \varphi_i q_{s2,i}\right)^3}$$

$$I_3 = \int_0^1 \frac{\varphi_j dx}{\left(1 - \sum_{i=1}^n \varphi_i q_{s2,i}\right)^2},\quad I_4 = \int_0^1 \frac{\varphi_j^2 dx}{\left(1 - \sum_{i=1}^n \varphi_i q_{s2,i}\right)^3} \tag{A1}$$

Appendix B

The coefficients appearing in Equations (21) are defined as:

$$S_1 = \sum_{i=1}^{n} \left\{ \int_0^1 \varphi_j{}' \varphi_i{}' dx \right\} q_{s1,i}, \quad S_2 = \int_0^1 \left(\sum_{i=1}^{n} \varphi_i' q_{s1,i} \right)^2 dx,$$

$$S_3 = \sum_{i=1}^{n} \left\{ \int_0^1 \varphi_j{}' \varphi_i{}' dx \right\} q_{s2,i}, \quad S_4 = \int_0^1 \left(\sum_{i=1}^{n} \varphi_i' q_{s2,i} \right)^2 dx, \tag{B1}$$

$$R_{11} = (K_2 + 2\alpha_1 S_1^2 + \alpha_1 S_2 K_3 - 2\alpha_2 V_c^2 I_2),$$

$$R_{12} = 2\alpha_2 V_c^2 I_2 , \qquad R_{21} = 2\alpha_2 V_c^2 I_2$$

$$R_{22} = \left(\alpha_4 K_2 + 2\alpha_5 S_3^2 + \alpha_5 S_4 K_3 + \alpha_7 \left(V_{p2} + V_{p1}\right) K_3 - 2\alpha_2 V_c^2 I_2 - 2\alpha_2 V_{dc}^2 I_4\right).$$